AN EXPERIMENTAL TEST-BED TO EVALUATE THE TOOL POSITIONING ERROR IN A REDUNDANT PARALLEL ROBOT FOR MILLING APPLICATIONS

Brian J. Auza Tarquino
Tarcisio A. Hess-Coelho
Departamento de Engenharia Mecatrônica e de Sistemas Mecânicos, Escola Politécnica da Universidade de São Paulo. Avenida Professor Mello Moraes nº 2231, CEP05508-900 - São Paulo-SP.
brianauza@usp.br
tarchess@usp.br

Abstract. *Serial mechanisms have been widely applied in industrial operations such as milling and positioning. On the other hand, in the last decades some investigations about parallel architecture have been also developed, due to the fact that they present some advantages in comparison with the serial. Fast motions, modular construction, lightness and high load capacity are some observed characteristics in pick-and-place parallel robots used in industry. Therefore, it is important to investigate and explore the performance of parallel mechanisms in different kind of operations where stiffness and precision are involved.*
In this manner, a parallel robot for milling applications was designed and constructed. Basically, it has only two axis for milling and its mechanical structure is fully modular. The topology of the parallel mechanism responsible for tool positioning corresponds to a planar redundant mechanism. In fact, it employs three active kinematic chains instead of only two.
In order to investigate the positioning static error and the robot structure stiffness, an experimental test-bed has been built. Then, measurements of the tool positioning error are conducted in two conditions: unloaded and loaded. After collecting these data, the static error map is plotted for the robot available workspace. The static error mapping allows the robot user to select the best configurations, during motion planning phase, in terms of milling quality.

Keywords: *Parallel robot, Milling machine, Didactic equipment.*

1. INTRODUCTION

During the last two decades, an increasing interest in parallel kinematic structures for machine-tool applications has been demonstrated by industry and academia (Gojtan, 2009). These structures are characterized by the presence of many independent kinematic chains actuating simultaneously on a moving platform. Fast dynamic response, lightness, modular construction, optimal stiffness possibilities and precision are some potential advantages of this kinematic architecture over the conventional serial counterpart. In spite of this potential, it becomes important to study stiffness and static error characteristics in order to explore and optimize its capabilities.

A parallel robot for milling applications was designed and constructed in recent works (Hartmann, V.N., Stipkovic-Filho, M., Hess-Coelho, 2013). According to the conceptual design, the mechanism should follow some fundamental directions such as being based on a tool positioning mechanism with parallel architecture, low structural complexity, a redundant kinematic chain and modular construction. The parallel mechanism has three identical limbs (*3PRR*), each one consists of an active linear joint and two rotational ones as shown in Fig. 1. This planar mechanism allows to position the tool at any coordinate point inside its workspace. Figure 1 indicates the adopted global reference system, *X*-axis directions will be referred as horizontal and *Y*-axis directions as vertical.

This work aims to evaluate the static error and the mechanism stiffness in some proposed configurations. Figure 2 shows the tool workspace and some proposed points for experimental and numerical analysis. A static model is also developed to study the influence of flexible active joints and links (Yoon, et al., 2004). Experimental tests follow some directions for compliance tests in robots (ANSI/RIA R15.05-1-1990).

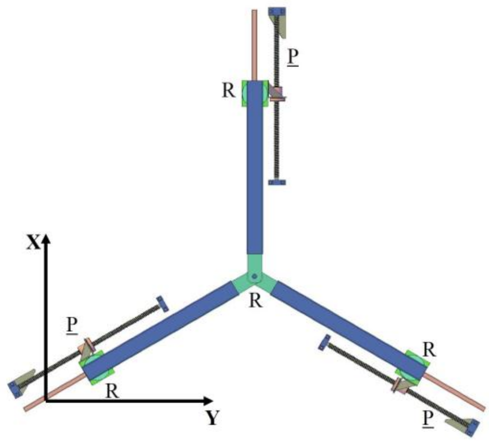

Figure 1. Mechanism joints and reference system

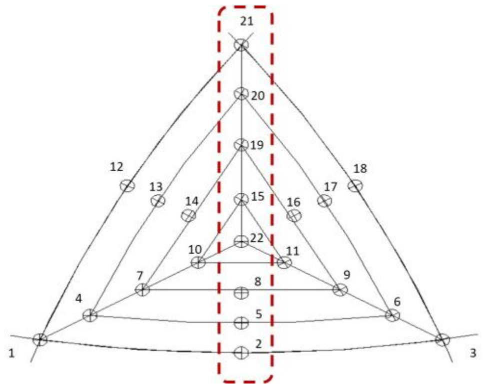

Figure 2. Workspace limits and proposed point for experimental and numerical procedures

2. EXPERIMENTAL AND NUMERICAL PROCEDURES FOR THE STATIC ERROR EVALUATION

2.1 Displacement measuring method

A Polytec Laser Doppler Vibrometer (LDV) was used as the measurement method, it consists of a OFV 323 sensor head and a OFV 3020 decoder, a National Instruments data acquisition board was also used for collecting data.

The LDV is an optical transducer used for determining velocity and displacement at a fixed point, it is based on the Doppler-effect by sensing the frequency shift of back scattered light from the moving surface. In this case, the displacement mode was used in order to perform static measurements. The analog signal varies between $16\ V_{p\text{-}p}$, and it is proportional to the measurement value by the set displacement range (d_r), all the tests were conducted with $d_r=640\ \mu m/V$. According to these parameters the LDV resolution is $2{,}6\ \mu m$ and the measurement range limit is $5\ mm$.

Figure 3 shows the acquisition dataflow, it begins by sensing the displacement variations with the laser beam. After this, the signal passes through a decoder in order convert the signal to an analog voltage value that is collected by the data acquisition board and finally sent to a computer.

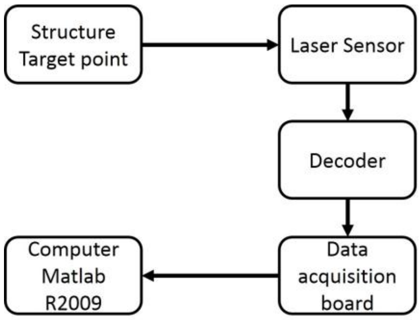

Figure 3. Acquisition dataflow

2.2 Load measurement method

A digital dynamometer was used to calibrate the incremental applied load, its resolution is $0.05\ kg_f$. This device works with a load cell and a display panel that records the measure.

2.3 Experiment setup

The experiment consists of the mechanism to be measure, load cell, load display panel, LDV system, data acquisition device, reflective band for the laser target and a computer with MatLab® program for signal treatment. In the case of horizontal loads (F_x) an additional mirror was used for reflecting the laser beam in perpendicular directions as noticed in Fig. 4.

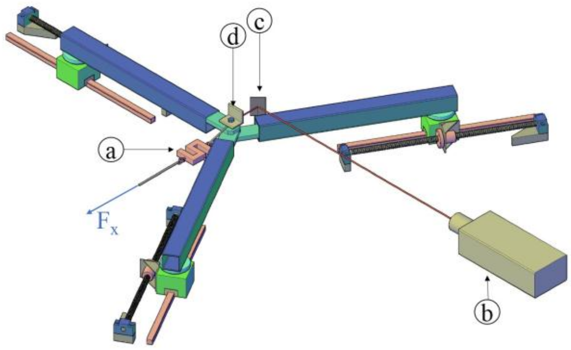

Figure 4. Experiment layout for the *X*-axis displacement measure, a) load cell, b) LDV, c) mirror and d) target with reflective band

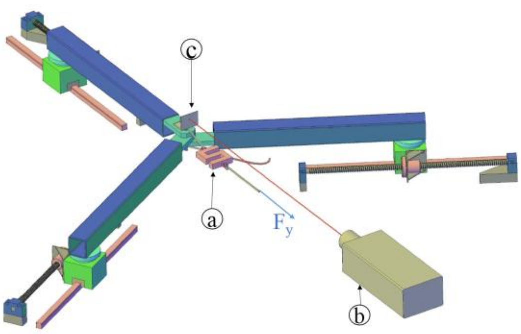

Figure 5. Experiment layout for the *Y*-axis displacement measure, a) load cell, b) LDV and c) target with reflective band

2.4 Experimental procedure

The introduction section proposes some points for developing the numerical model, in this section eight of those points were considered for experimental observations. These points belong to the vertical middle line of the workspace, Figure 2 highlights these points numbered as *2, 5, 8, 22, 15, 19, 20* and *21*.

The first step was setting up the mechanism configuration and locating the tool at each proposed point. Then the LDV beam was targeted to a reflective band located at the tool point in order to measure displacement variations. After that, a decreasing load was applied from 50 *to* $0\ kg_f$. For some values of the decreasing force applied, a signal acquisition program was run and measuring data was collected for later treatment and interpretation. This operation was repeated for each experimental point in two situations, a vertical load which is parallel to the *Y* axis and a horizontal load that is parallel to the *X* axis.

2.5 Numerical Model

The model consists of positional kinematics and finite element method analysis according to the static diagram and geometric characteristics presented in Figures 6 and 7. Equations 1, 2 and 3 show some geometric relations between the mechanism parameters and positional variables, with these relations is possible to determine the node coordinates for each proposed mechanism configuration and tool positioning along the workspace. The reference system is the same used in the introduction section, the *(x, y)* coordinates correspond to the tool position as noticed in Fig. 6.

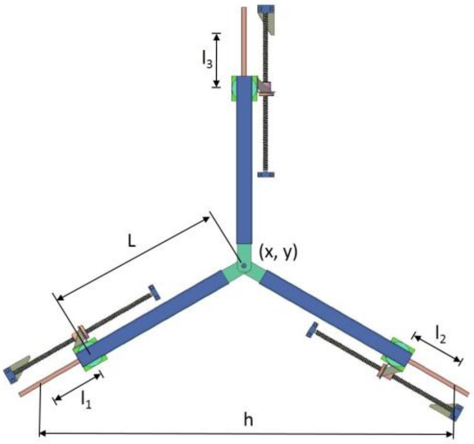

Figure 6. Mechanism geometric parameters

A rod element was adopted because all nodes represent rotational joints with two degrees of freedom in plane. The linear springs in Fig. 7 intend to model flexible prismatic joints with different stiffness values for each direction. K_b represents the bearing radial stiffness constant reported by the manufacturer and K_j is the prismatic joint stiffness constant in the linear actuator direction.

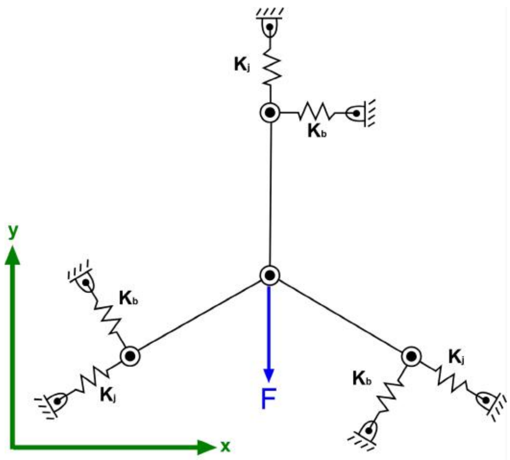

Figure 7. Mechanism model for numerical static error analysis

$$\left(x-\frac{\sqrt{3}}{2}l_1\right)^2 + \left(y-\frac{l_1}{2}\right)^2 = L^2 \quad (1)$$

$$\left(x-h+\frac{\sqrt{3}}{2}l_2\right)^2 + \left(y-\frac{l_2}{2}\right)^2 = L^2 \quad (2)$$

$$\left(x-\frac{h}{2}\right)^2 + \left(y-\frac{\sqrt{3}}{2}h+l_3\right)^2 = L^2 \quad (3)$$

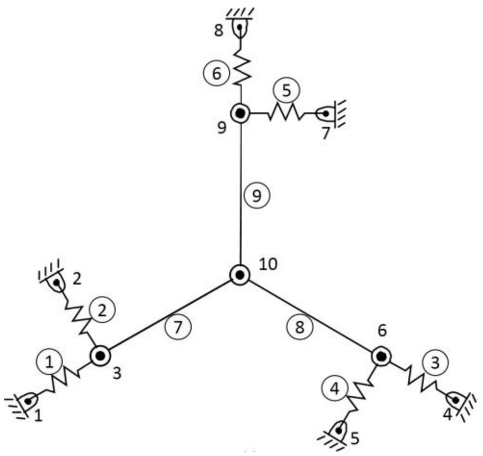

Figure 8. Plane truss model

Figure 8 shows the nodal distribution for structural finite element analysis, the rounded numbers represent the element numeration. Equation 4 relates external forces *[F]* with nodal displacements and global stiffness matrix, which is obtained by assembling each element local stiffness matrix as shown in Equation 6. The *{d}* array represents de nodal displacements in global reference system. The single element stiffness matrix *[k]* contains element material and geometric properties, *A* is the cross section, *L* represents the element length and *E* the Young modulus.

$$F = K \quad d \tag{4}$$

$$k = \frac{AE}{L}\begin{bmatrix} 1 & -1 \\ -1 & 1 \end{bmatrix} \tag{5}$$

$$K = \sum_{e=1}^{N} \left[\hat{k} \right] \tag{6}$$

In order to solve kinematic and nodal displacements for all the 22 proposed mechanism configurations, a program script was developed in MatLab® following the diagram in Fig. 9.

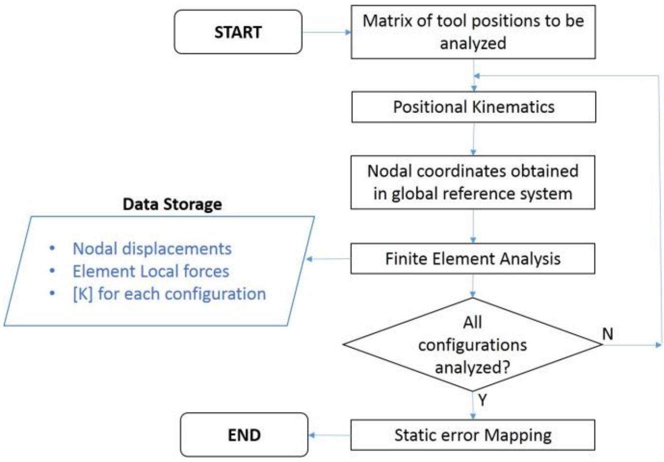

Figure 9. Script diagram for static error Mapping

3. EXPERIMENTAL AND NUMERICAL RESULTS

Figure 10. Experiment Layout

Figure 10 shows the mechanism experimental test-bed, the LDV and a digital dynamometer calibrating a Y-axis force (F_y).

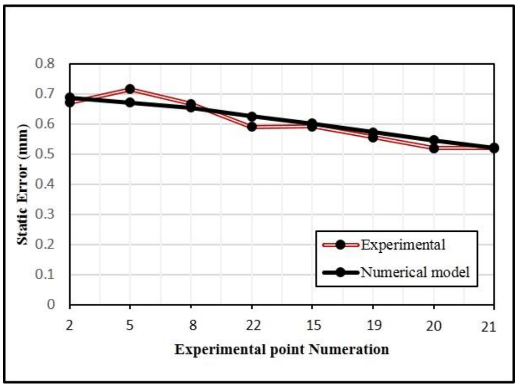

Figure 11. Static error with *Y*-axis force of *50 kg$_f$ (490,5 N)*

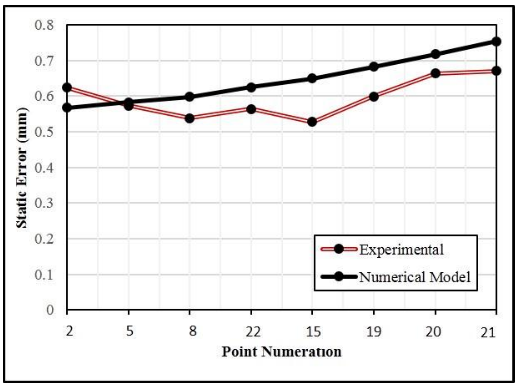

Figure 12. Static error with *X*-axis force of *50 kg$_f$ (490,5 N)*

Figures 11 and 12 show the experimental static error compared to numerical model results for the mentioned points in section 2.4. The adopted point numeration sequence corresponds to geometrical position along the workspace. Results in Fig. 11 show the tool displacement variations along the *Y* axis while a vertical load of *50 kg$_f$* is applied, a similar situation could be observed in Fig. 12 whereas horizontal loads and displacements take place.

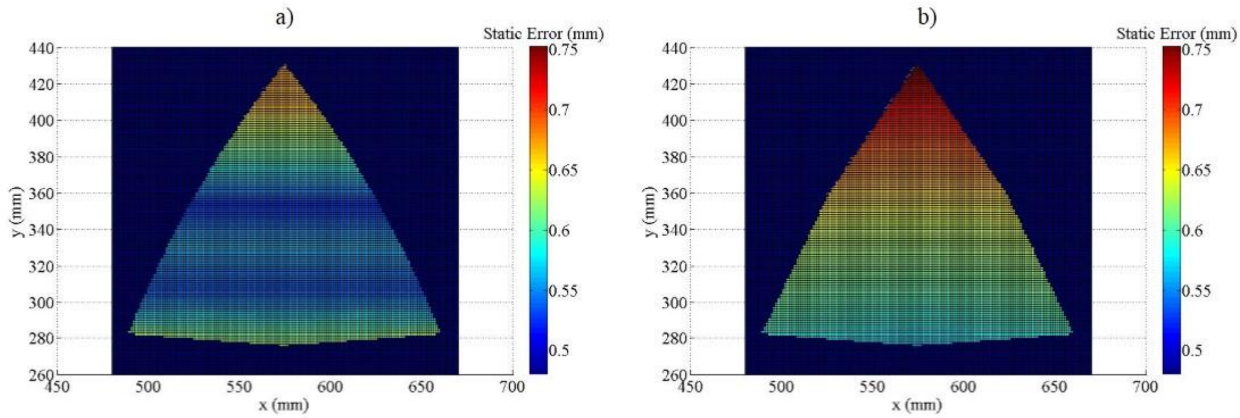

Figure 13. Static error mapping for the horizontal force of *50 kg$_f$ (490,5 N)*, a) Experimental, b) Numerical Model

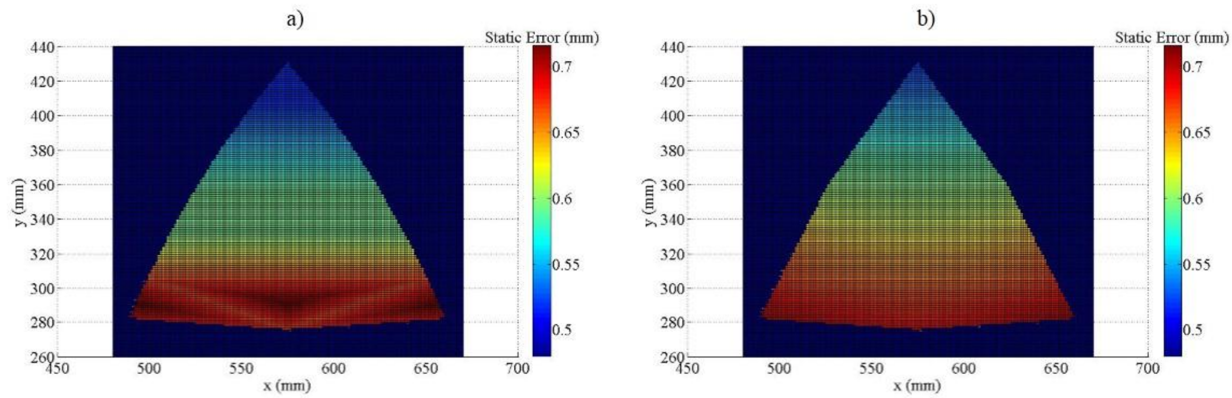

Figure 14. Static error mapping for the vertical force of *50 kg$_f$ (490,5 N)*, a) Experimental, b) Numerical Model

Figures 13 and 14 compare the experimental and numerical static error along the workspace in two loading situations previously described.

4. DISCUSSIONS

The numerical model allowed to estimate an approximate K_j value for the mechanism prismatic joints, Figures 11 and 12 display experimental results and the numerical model was adjusted according to this behavior. In Figures 13 and 14, this estimated value ($K_j=525$ *N/mm*) was used to obtain a complete numerical map by extending the mathematical model to all 22 points presented in Fig. 2.

Even though in Fig. 12 some discrepancy could be observed, the magnitude of the static error remains approximate. There were experimental factors that could have influenced these results such as the difficulty of positioning the reflecting mirror shown in Fig.4, while results in Fig. 11 were obtained by a direct measure without using any mirror, as displayed in Fig. 5. The influence of this discrepancy factor could also be noticed in Fig. 13. The adopted radial stiffness value was extracted from the manufacturer's catalogue, $K_b = 9800$ *N/mm* (NSK Rolamentos, 2013).

5. CONCLUSIONS

The experimental procedure suggests that K_j has a relevant influence over the mechanism stiffness in all configurations, it could be important to study the individual prismatic joint stiffness for optimizing the static error magnitude. K_j also suggests that its value is influenced not only by the bearing deformation.

In future works, a more complete model could also be developed in order to contemplate spatial displacements and moments that are not probably considered in the present study.

The error map shows more significant values in regions close to singular mechanism configurations as it was previously studied (Hartmann, V.N., Stipkovic-Filho, M., Hess-Coelho, 2013). Even though present numerical results vary in magnitude compared with the previous work, the static error behavior and the trends of variation along the workspace remain similar. The effect of flexible active joints, which was not contemplated in the previous work, influenced to higher magnitudes of static error.

6. REFERENCES

ANSI/RIA R15.05-1-1990, 1990. *Point-to-Point and Static Performance Characteristics*. American National Standards Institute, New York.

Daryl L. Logan, 2007. *A First Course in the Finite Element Method*. University of Wisconsin-Platteville, Fourth Edition.

G.E.E. Gojtan, 2009. *Análise da precisão de uma estrutura robótica com cinemática paralela assimétrica de topologia 2UPS+PRP, em função do mapeamento dos erros de posicionamento da plataforma móvel no espaço disponível, durante operação de fresamento de acabamentoaplicando modelagem matemática*. Escola Politécnica da Universidade de São Paulo. Departamento de Engenharia Mecatrônica e de Sistemas Mecânicos.

Hartmann, V.N., Stipkovic-Filho, M., Hess-Coelho, T.A. and Almeida, S.L.R 2013. *'Development os milling parallel robot for educational purposes'*, Int. J. Mechanism and Robotic Systems.

Lun-Wen Tsai, 1999. *Robot Analysis: The Mechanics of Serial and Parallel Manipulators.* John Wiley & Sons, New York.

NSK, 2013 . *Rolamentos.*

Yoon, W. K., Suehiro, T., Tsumaki, Y. and Uchiyama, M., 2004, *"Stiffness Analysis and Design of a Compact Modified Delta Parallel Mechanism"*, Robotica, vol. 22, pp. 463-475.

7. RESPONSIBILITY NOTICE

The authors are the only responsible for the printed material included in this paper.